Journal of Renewable Materials

Tech Science Press

DOI: 10.32604/jrm.2024.049068

ARTICLE

Synergism of Zinc Oxide/Organoclay-Loaded Poly(lactic acid) Hybrid Nanocomposite Plasticized by Triacetin for Sustainable Active Food Packaging

Ponusa Songtipya[1,2,*], Thummanoon Prodpran[1,2], Ladawan Songtipya[1,2] and Theerarat Sengsuk[1]

[1]Center of Excellence in Bio-Based Materials and Packaging Innovation, Faculty of Agro-Industry, Prince of Songkla University, Hat Yai, Songkhla, 90110, Thailand

[2]Food Packaging Technology Program, Faculty of Agro-Industry, Prince of Songkla University, Hat Yai, Songkhla, 90110, Thailand

[*]Corresponding Author: Ponusa Songtipya. Email: ponusa.j@psu.ac.th

Received: 26 November 2023 Accepted: 28 February 2024 Published: 17 July 2024

ABSTRACT

The synergistic effect of organoclay (OC) and zinc oxide (ZnO) nanoparticles on the crucial properties of poly (lactic acid) (PLA) nanocomposite films was systematically investigated herein. After their incorporation into PLA via the solvent casting technique, the water vapor barrier property of the PLA/OC/ZnO film improved by a maximum of 86% compared to the neat PLA film without the deterioration of Young's modulus or the tensile strength. Moreover, the film's self-antibacterial activity against foodborne pathogens, including gram-negative (*Escherichia coli*, *E. coli*) and gram-positive (*Staphylococcus aureus*, *S. aureus*) bacteria, was enhanced by a maximum of approximately 98–99% compared to the neat PLA film. Furthermore, SEM images revealed the homogeneous dispersion of both nano-fillers in the PLA matrix. However, the thermal stability of the film decreased slightly after the addition of the OC and ZnO. The film exhibited notable light barrier properties in the UV-Vis range. Moreover, the incorporation of a suitable biodegradable plasticizer significantly decreased the T_g and notably enhanced the flexibility of the nanocomposite film by increasing the elongation at break approximately 1.5-fold compared to that of the neat PLA film. This contributes to its feasibility as an active food packaging material.

KEYWORDS

Poly(lactic acid) nanocomposite; organoclay; zinc oxide; barrier property; antibacterial activity; active food packaging

1 Introduction

Sustainable food packaging is taking on an increasingly important role in retarding the deterioration of packaged food products and ensuring food safety. Such packaging involves less energy and material input; fewer negative social, economic, and environmental impacts; and minimized municipal solid waste generation [1]. The selection of renewable environmentally friendly polymers as food contact materials is one of the potential factors contributing to more sustainable packaging in the food supply chain [2].

Poly(lactic acid) (PLA) is considered a promising and growing alternative to conventional petroleum-based polymers for packaging and is presently widely used in this regard. Briefly, PLA is a linear aliphatic thermoplastic polyester primarily synthesized from renewable agricultural resources, such as

sugar beet, corn, soy protein, potato, and biomass waste. It exhibits biocompatibility and biodegradability and possesses unique features, such as low toxicity, high transparency, and environmentally benign characteristics. Additionally, PLA is classified as "generally recognized as safe" (GRAS) for use as a food contact polymer by the U.S. Food and Drug Administration (FDA). However, its drawbacks, such as intrinsic chain rigidity (resulting in high brittleness), low gas barrier properties, and poor crystallization behavior, need to be addressed to increase its applicability, specifically in the food packaging industry [3].

Nanotechnological advances, specifically in the polymer nanocomposite field, have led to the use of low nano-filler contents compared with the case for neat and conventional polymer composites. As such, these advances have the potential to enhance the properties of polymers and provide new functionalities [4]. Due to their abundance, low costs, high cation exchange capacity, high aspect ratio, high strength and stiffness, and thermal stability, nanoclays can act as nano-fillers to improve the functional (e.g., thermomechanical, optical, rheological, and barrier) properties of polymers [5]. They can function as a nucleating agent, facilitating the crystallization process and improving the mechanical and physical properties of crystalline polymers [6–8]. Furthermore, nanocomposite dispersion can be improved by enhancing the affinity between the nanoclay layers and the organophilic polymer via simple organic modifications. Cloisite 30B, a natural montmorillonite organoclay (OC) mineral consisting of an organic diol in the inter-galleries, promotes favorable intermolecular interactions with the carbonyl functional group of PLA, resulting in significant intercalation of the PLA chains into the interlayer spaces of OC [1]. According to Kalendova et al., incorporating OCs into PLA increases the barrier property of the film [9]. Moreover, Rhim and coworkers have reported that OC exhibits antimicrobial activity against *Listeria monocytogenes* in the PLA/OC composite film, with a slight decrease in the water vapor permeability [10].

Additionally, zinc oxide (ZnO), generally recognized as a safe (GRAS) material by the FDA, is a notably promising nano-filler material and of great interest as an antimicrobial compound. It is applied as a food packaging material due to its nontoxic nature (at the optimal amounts used), broad range of antimicrobial efficacy, UV absorption properties, simple synthesis, and widespread availability and affordability [11]. Marra et al. reported that the addition of ZnO to PLA notably reduces the growth of *E. coli* by 99.99%, though the nanocomposite film slightly increases the water vapor permeability [12]. In another study, although displaying high inhibitory efficacy against *E. coli*, *S. aureus*, and *Klebsiella pneumoniae*, PLA/ZnO nanocomposite films exhibit inferior mechanical properties due to poor molecular interactions between ZnO and PLA [13]. Recently, an alternative, simpler approach has been documented by incorporating ZnO-deposited nano-fillers, such as ZnO-deposited halloysite nanotubes [14] and cellulose nanocrystals [15,16], into PLA. Moreover, hybrid structures of OCs and metal oxides have been previously reported for different polymer matrices. Rodolfo and coworkers developed poly(vinyl chloride) in the presence of OCs and metal oxides ($CuO/MoO_3/ZnO$) [17], and in a recent study, Muiz et al. reported on a silver-ZnO-OC-reinforced chitosan nanocomposite [18]. These studies have revealed the excellent comprehensive properties of nanocomposites resulting from the synergistic action of nano-fillers. Not only do the nano-fillers enhance the mechanical properties–specifically, Young's modulus and the tensile strength–of the composites, but they also improve their antimicrobial ability and UV-shielding performance. However, the elongation at break of these nanocomposite films was decreased, limiting their applicability.

To the best of our knowledge, the incorporation of OC/ZnO into PLA has not been previously reported. Thus, this study focused on developing flexible hybrid PLA/OC/ZnO nanocomposite films and investigating the synergistic effect of OC/ZnO on their mechanical, thermal, and barrier properties. In addition, the antibacterial activity of the films was compared to that of PLA/OC and neat PLA films. The brittleness and rigidity of the PLA nanocomposite films were overcome by adding an appropriate amount of a selected bio-based plasticizer derived from renewable sources, triacetin (TA), contributing to the applicability of the films in food packaging. TA, also known as glyceryl triacetate, is classified as a

GRAS human food ingredient by the FDA [19]. It can be synthesized via acetylation reaction of crude glycerol, a by-product of biodiesel, with acetic acid in the aiding of appropriate catalysts. TA is also a common additive used in the cosmetics, pharmaceutical and food products [20].

2 Materials and Methods

2.1 Materials

PLA (4032D, M_n = 88,500 g/mol and M_w/M_n = 1.8) was procured from Nature Work Co., Ltd. (Blair, NE, USA). Nano-ZnO powder (with an average particle size of 25–50 nm) was provided by the College of Nanotechnology (King Mongkut's Institute of Technology Ladkrabang, Thailand). The OC, Cloisite 30B, with a cation exchange capacity (CEC) of 90 meq/100 g of clay and a density of 0.2283 g/cm^3, was supplied by BYK Additives, Inc. (USA). The OC had an average particle size of 7 μm, as reported by the supplier. The substituted cation of Cloisite 30B is known as bis-(2-hydroxyethyl) methyl (hydrogenated tallow alkyl) quaternary ammonium. Reagent-grade chloroform, glutaraldehyde solution, ethanol, and TA ($C_9H_{14}O_6$) were purchased from Sigma-Aldrich (St. Louis, MO, USA). Luria–Bertani (LB) agar and phosphate-buffered saline (PBS) were acquired from HiMedia Laboratories Pvt., Ltd. (India). All materials were used as received without further modification.

2.2 Microorganisms

The common foodborne pathogenic bacteria used in this study were *E. coli*, AGM-BE, and *S. aureus*, AGM-BS3. All strains were obtained from the Faculty of Agro-Industry, Prince of Songkla University, Thailand.

2.3 Preparation of PLA and PLA Nanocomposite Films

PLA film was prepared via the solvent casting technique modified from the study by Rhim et al. [10]. Briefly, 5% (w/v) PLA was dissolved in chloroform while stirring continuously at room temperature. The resulting solution was then applied onto a glass plate and dried at room temperature. The film was peeled and further dried overnight at 60°C in a vacuum oven to remove the remaining solvent to prevent the plasticization effect. In preparing the PLA/OC nanocomposite film, a predetermined amount of 5 wt% OC was dispersed in chloroform by vigorous stirring for 1 h at room temperature, followed by sonication for 15 min. The OC suspension was then mixed with the prepared PLA solution, sonicated for 15 min, casted onto the glass plate, and left to dry at room temperature. The PLA/OC/ZnO films were prepared by adding ZnO at 1, 3, and 5 wt% to the OC suspension and then combining this mixture with the prepared PLA solution.

The films with the TA plasticizer were prepared by mixing the prepared PLA/OC5/ZnO5 suspension (containing 5 wt% of both the OC and ZnO) with solutions containing TA contents of 10 and 20 wt% [19]. Table 1 presents the compositions and associated designations of the neat PLA and PLA nanocomposites.

Table 1: Compositions and designations of the PLA and PLA nanocomposite films

Designation	OC (wt%)	ZnO (wt%)	TA (wt%)
PLA	0	0	0
PLA/OC5	5	0	0
PLA/OC5/ZnO1	5	1	0
PLA/OC5/ZnO3	5	3	0
PLA/OC5/ZnO5	5	5	0
PLA/OC5/ZnO5/TA10	5	5	10
PLA/OC5/ZnO5/TA20	5	5	20

2.4 Mechanical Properties

The mechanical properties of the films were quantified by stress–strain measurements at room temperature using a universal testing machine (Tinius Olsen, H10KS, USA) in accordance with ASTM Method D 882-88. The specimens were conditioned at 25°C and 50% relative humidity (RH) in an environmental chamber for 48 h before testing. The initial grip separation was set to 50 mm. Young's modulus, the tensile strength, and the elongation at break were then measured at the crosshead speed of 50 mm/min. Five specimens of each sample were used to obtain average values.

2.5 Water Vapor Permeability (WVP)

The water vapor permeability (WVP) was measured using a slightly modified version of the ASTM E96-92 test methods. Aluminum permeation cups were filled with dried silica gel (0% RH) and sealed with the films using silicone vacuum grease. The cups were placed in a desiccator at 30°C containing distilled water, and the weight gain of the cups was determined every hour for a total of 8 h. The WVP of the films was calculated as per Eq. (1):

$$WVP\left(gm^{-1}s^{-1}Pa^{-1}\right) = wlA^{-1}t^{-1}(P_2 - P_1)^{-1}, \tag{1}$$

where w is the weight gain of the cup (g), l is the film thickness (m), A is the exposed area of the film (m^2), t is the time of weight gain (s), and $(P_2 - P_1)$ is the vapor pressure difference across the film (Pa). Three film samples were used for WVP testing.

2.6 Antibacterial Activity

The antibacterial activities of the films were investigated against *S. aureus* and *E. coli* using the shake flask method according to previously published work [15]. First, the sterilized film (0.1 g) was immersed into 5 mL of the bacterial suspension (10^6 CFU/mL) and incubated at 37°C at 200 rpm for 48 h. After that, the solution was diluted successively, and LB agar was inoculated with 100 μL of each dilution using the spread plate method. The glass plates were incubated at 37°C for 24 h, and photographs were taken with a digital camera. For the quantitative analysis, the bacterial growth inhibition was calculated at 0, 12, 24, and 48 h using Eq. (2):

$$\text{Growth inhibition } (\%) = \frac{A_0 - A}{A_0} \times 100, \tag{2}$$

where A_0 and A represent the number of colonies for the PLA control and the nanocomposite sample, respectively. Three replicates were carried out for each sample.

2.7 Bacterial Morphology

Bacterial adhesion was carried out by sedimentation, using the procedure described by Kammoun et al. with some modifications [21]. The film samples and a glass slide were immersed in a bacterial solution (10^6 CFU/mL) and incubated at 37°C for 12 h to allow for bacterial adhesion. Thereafter, the bacterial suspension was removed with a pipette. Next, 2.5% glutaraldehyde was added to fix the adherent bacteria at a temperature of 4°C for 2 h. Dehydration with an increasing gradient of ethanol (25%, 50%, 80%, 90%, and 100% v/v) was performed separately after removing the glutaraldehyde solution. The critical point drying (CPD) technique was used to dry the bacterial cells, and the samples were sputter-coated with gold. Morphological changes of the bacteria were observed using scanning electron microscopy (SEM) (Hitachi, SU3900, Japan), and bacteria with no sample treatment were used as a control.

2.8 Color and Light Transmission

The color parameters–lightness (L*, light/dark), redness (a*, red/green), and yellowness (b*, yellow/blue)–of PLA and its nanocomposite films were measured via the CIE L*a*b* system using a colorimeter

(Hunterlab, Reston, VA, USA). The index of the total color difference (ΔE*) was calculated according to Eq. (3). The results were averaged over at least five replications.

$$\Delta E^* = \sqrt{(\Delta L^*)^2 + (\Delta a^*)^2 + (\Delta b^*)^2}, \quad (3)$$

where ΔL*, Δa*, and Δb* are the differences between the corresponding color parameter of the sample and the white standard (L* = 92.83, a* = −1.32, and b* = 0.56).

A UV-Vis spectrophotometer (UV-1800, Shimadzu, Kyoto, Japan) was used to characterize the light transmittance of five replicates for each film sample over a scan range of 200 to 800 nm.

2.9 Film Morphology

The surface and cross-sectional morphology of the selected film samples were visualized using SEM (Hitachi, SU3900, Japan). For cross-sectional visualization, the samples were fractured using liquid nitrogen. The samples were mounted on a bronze stub, sputtered with gold particles (Sputter Coater SPI-Module, PA, USA) for conductivity purposes, and characterized at the acceleration voltage of 20 kV.

2.10 Differential Scanning Calorimetry (DSC)

Differential scanning calorimetry (DSC) analysis was carried out using a Mettler-Toledo DSC3+ under a nitrogen atmosphere. The samples (3–10 mg) were first heated from 25°C to 200°C at a heating rate of 10°C/min. To eliminate the anterior thermal history of the samples, an isothermal process was conducted at this temperature for 3 min. Subsequently, the samples were cooled to 25°C. A second heating scan from 25 to 200°C at 10°C/min was then used to characterize the glass transition temperature (T_g), cold crystallization temperature (T_{cc}), melting temperature (T_m), and the degree of crystallinity (X_c) of the samples. X_c was calculated according to Eq. (4) as follows:

$$X_c(\%) = \frac{\Delta H_m - \Delta H_{cc}}{\Delta H_m^0 \times (1 - x)} \times 100, \quad (4)$$

where ΔH_m is the enthalpy of melting (J/g), ΔH_{cc} is the enthalpy of cold crystallization (J/g), ΔH_m^0 is the theoretical enthalpy of melting of the full crystallization of PLA (93.7 J/g) [22], and x is the weight fraction of the filler.

2.11 Thermal Gravimetric Analysis (TGA)

The thermal stability of PLA and selected nanocomposite films (PLA/OC5/ZnO5 and PLA/OC5/ZnO5/TA10) was characterized by thermal gravimetric analysis (TGA; TGA8000, Perkin Elmer, USA). The temperature ranged from 30°C to 800°C, and a heating rate of 10°C/min was employed under a nitrogen atmosphere.

2.12 Statistical Analysis

All analyzed data were presented as the mean ± standard deviation. The significance of the differences between the data was determined using a one-way analysis of variance (ANOVA). The values of the significant difference and mean were obtained by performing Duncan's test at a confidence level of $p < 0.05$.

3 Results and Discussion

3.1 Mechanical Properties

Fig. 1 shows the mechanical properties of the PLA nanocomposite films compared with the neat PLA film (control). The addition of OC and ZnO led to a pronounced improvement in the stiffness of the PLA film. The incorporation of 5 wt% of OC increased the Young's modulus (YM) of the PLA film from 1228 to

1562 MPa (Fig. 1a). Furthermore, a greater enhancement was observed for PLA/OC/ZnO, with the YM value increasing twofold ($p < 0.05$; PLA/OC5/ZnO3 and PLA/OC5/ZnO5) compared to the neat PLA film. These YM values were higher than that of the low-density polyethylene (LDPE) film (approximately 300 MPa) presented by Giannakas et al. [23]. The increase in YM was expected and corroborates published results: the high rigidity induced by the incorporation of the OC and ZnO nano-fillers resulted in the suppression of chain movement [24].

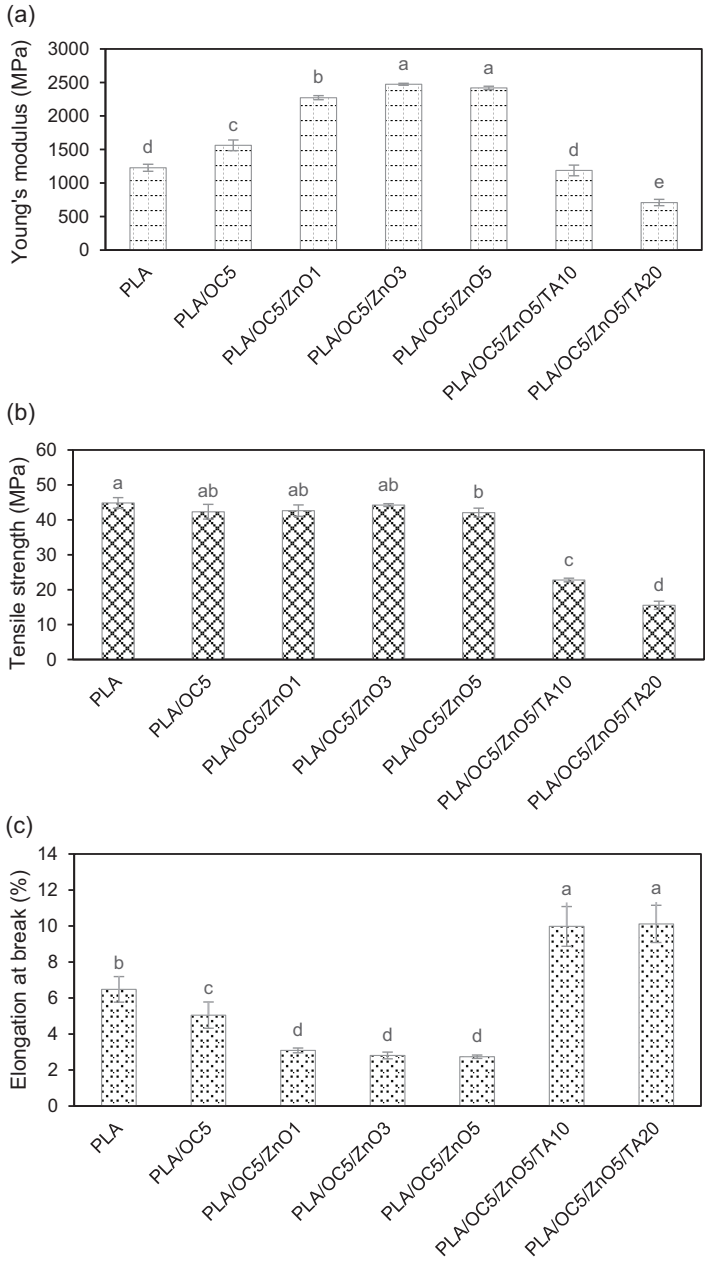

Figure 1: Mechanical properties of PLA and its nanocomposites: (a) Young's modulus (YM), (b) tensile strength (TS), and (c) elongation at break (EB). Different lowercase letters indicate the significant difference ($p < 0.05$)

The tensile strength (TS) did not change significantly when both the OC and ZnO were added (Fig. 1b). Strong interactions between the nano-fillers and the PLA matrix ultimately led to homogeneous dispersion and might play a key role in controlling the mechanical strength [25]. Specifically, the diols in the organic surfactant present in the OC exhibited a favorable enthalpic interaction with the C=O bonds in PLA, leading to the uniform dispersion of the OC layer [26,27]. After the addition of ZnO, particles of ZnO were deposited onto the OC via the binding of ZnO in the Si-O-Al region on the clay particle edges. This avoids a high degree of aggregation, a factor that led to the phase separation of PLA and ZnO, as documented in previous findings [14,28]. Therefore, the stress was effectively transferred, and the TS remained unchanged. The TS values range from 42–44 MPa and were comparable to those of conventional thermoplastic films, such as low-density polyethylene (LDPE), high-density polyethylene (HDPE), polypropylene (PP), and polystyrene (PS), ranging from 12–83 MPa [10,23].

The elongation at break (EB) values displayed a downward trend and an apparent correlation with the addition of OC and OC/ZnO (Fig. 1c). The lowest EB was observed for the PLA/OC5/ZnO5 film, approximately 50% lower ($p < 0.05$) compared with that of PLA. However, there was no statistically significant difference among the various ZnO compositions (1, 3, and 5 wt%). This declining tendency of the EB might be due to lower PLA chain mobility resulting from the reinforcing and/or restricting effect of the nano-fillers [14]. To improve the EB with regard to further applications, the plasticizer TA was added to the PLA/OC5/ZnO5 nanocomposite film to optimize the water vapor barrier and antibacterial activity.

TA reduced both the YM and TS of the PLA/OC5/ZnO5 film while greatly enhancing its EB (Fig. 1). Nevertheless, the EB of the plasticized PLA/OC5/ZnO5 film was still lower (by approximately 50%) than that of a previously reported LDPE film [23]. The addition of 10 wt% TA reduced the YM and TS by approximately 50% and 46%, respectively, compared with the PLA/OC5/ZnO5 film. At a higher content of TA (20 wt%), both the YM and TS decreased slightly. Furthermore, after the addition of TA, the EB values showed significant improvement by up to 270% compared with the PLA/OC5/ZnO5 film, regardless of the amount of TA added. This result agrees with the outcomes of a previous report suggesting that the TS and modulus values decreased while the EB increased due to the plasticizing effect of TA. The presence of TA could weaken the interaction between the PLA molecular chains and hinder polymer inter-chain interactions, facilitating the movement of the molecular chains [19]. This might be attributed to the interactions between the hydroxyl groups from TA and the carboxyl groups of the PLA. This would, therefore, led to a significant decrease in the YM and TS of the films.

3.2 Water Vapor Permeability (WVP)

PLA showed the highest WVP value of 1.57×10^{-11} gm^{-1} s^{-1} Pa^{-1}. Here, after incorporating OC (5 wt%) into the PLA, the water vapor barrier property significantly improved by 53% ($p < 0.05$; Fig. 2). Moreover, by incorporating and increasing the amount of ZnO, the WVP continuously decreased. The greatest improvement in the barrier property occurred at the highest amount of ZnO (5 wt%) in the PLA/OC5/ZnO5 sample, which exhibited a WVP reduction of 86% compared to the neat PLA film. The OC layer and ZnO dispersion increased the diffusion pathway length in the PLA matrix, increasing the difficulty for traveling water vapor molecules to diffuse through the PLA film [10,13,29]. In addition, Darie et al. reported that OC incorporation could increase the hydrophobicity of the PLA matrix, which was confirmed by increase in the contact angle value. Rhim et al. also reported similar findings. These factors consequently led to a reduction in the WVP [10,30]. The TA content affected the WVP of the PLA/OC5/ZnO5 film, which decreased slightly after the addition of 10 wt% TA while increasing after adding 20 wt% TA. This might be due to the good compatibility achieved after adding a small amount of TA. However, all nanocomposite films exhibited a lower WVP than the neat PLA film. This enhancement in the water vapor barrier property was important in food packaging films because their RH could significantly influence microbial growth, reducing the shelf life of the packed food products [13].

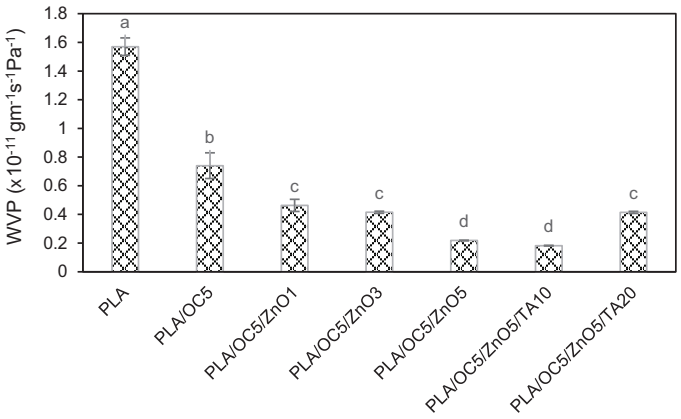

Figure 2: WVP of PLA and its nanocomposite films. Different lowercase letters indicate the significant difference ($p < 0.05$)

3.3 Antibacterial Activity

The antibacterial activity against both gram-negative (*E. coli*) and gram-positive (*S. aureus*) bacteria was investigated via colony counting; the results were quantified as the percentage of inhibition, as shown in Figs. 3 and 4. After 48 h of bacterial contact with the PLA and nanocomposite films, the neat PLA film did not inhibit the growth of the tested bacteria, while the PLA/OC5 film reduced the growth by approximately 16% ($p < 0.05$) for both *S. aureus* and *E. coli*. This might result from the presence of a quaternary ammonium cationic surfactant—methyl, tallow, bis-2-hydroxyethyl quaternary ammonium chloride (MT2EtOH)—in the OC, inhibiting bacterial growth [31]. This result agrees with findings reported in the literature [10]. Interestingly, the incorporation of both OC and ZnO led to synergistic performance. As expected, the antibacterial efficiency increased with increasing ZnO loadings due to the greater availability of active species on the nanocomposite. The PLA/OC5/ZnO5 film thus had the most prominent antibacterial effect, reducing the growth by 98% and 99% ($p < 0.05$) for *S. aureus* and *E. coli*, respectively, compared to the neat PLA film [32]. TA addition did not affect the antibacterial activity of the nanocomposite film. The proposed antimicrobial performance of ZnO might be due to (i) the generation of reactive oxygen species (ROS) resulting from photocatalytic activity, (ii) the formation of Zn^{2+} antimicrobial ions, and (iii) electrostatic interactions [14]. These mechanisms possibly inactivated vital proteins, disable DNA replication, and ultimately destroyed the bacterial cells by affecting their metabolic activity [11,33,34].

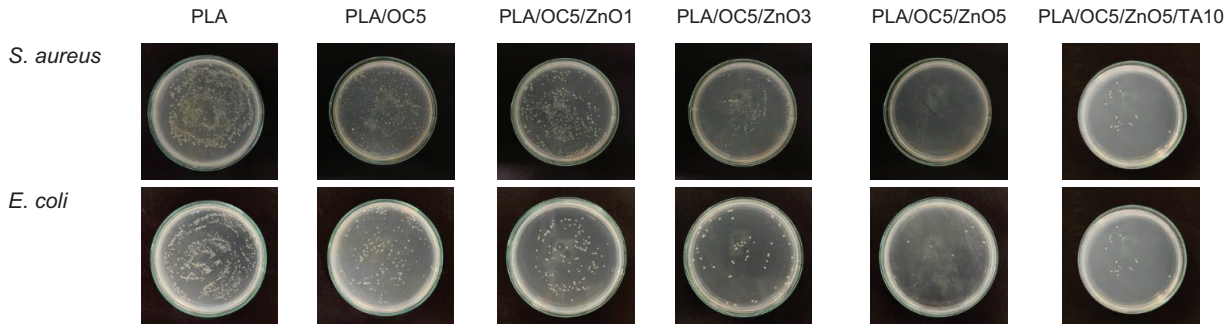

Figure 3: Formation of bacterial colonies; and antibacterial activity against *S. aureus* and *E. coli* for neat PLA, PLA/OC5, PLA/OC5/ZnO1, PLA/OC5/ZnO3, PLA/OC5/ZnO5, and PLA/OC5/ZnO5/TA10

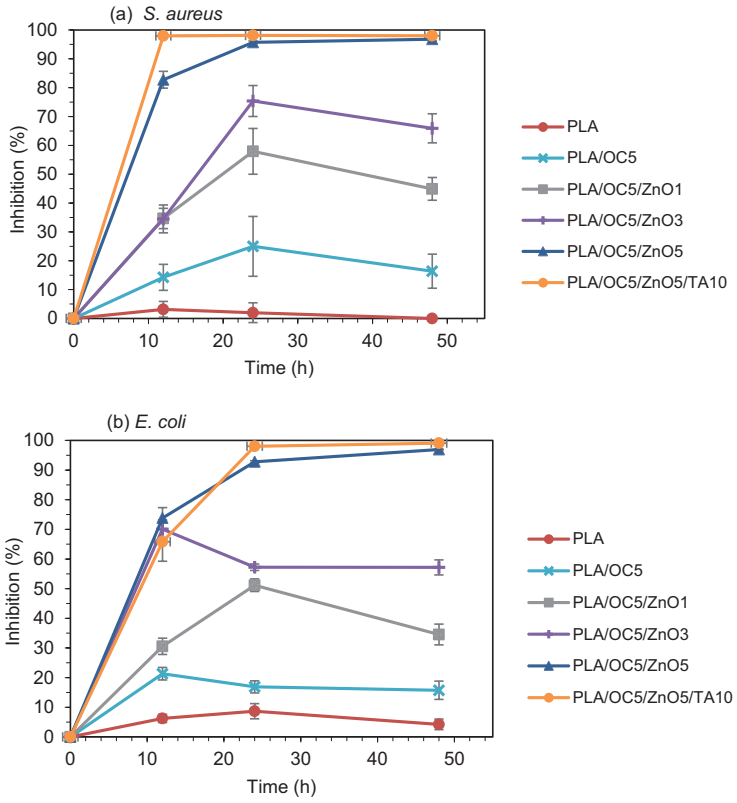

Figure 4: Inhibition of (a) *S. aureus* and (b) *E. coli* in contact with neat PLA, PLA/OC5, PLA/OC5/ZnO1, PLA/OC5/ZnO3, PLA/OC5/ZnO5, and PLA/OC5/ZnO5/TA10 for 12, 24, and 48 h

The bacterial cell morphology of *S. aureus* was investigated via SEM, indicating that the original *S. aureus* species was round-shaped, as depicted in Fig. 5a. After treatment with PLA/OC5/ZnO5, the cell wall and membrane rupture, and the subsequent leakage of cell contents resulted in bacterial surface damage and a distorted cell structure (red arrow), as shown in Fig. 5b. Therefore, one could state that the synergistic effect of OC and ZnO on the bacterial cells accounted for the remarkable antimicrobial efficacy of the PLA/OC5/ZnO5 film.

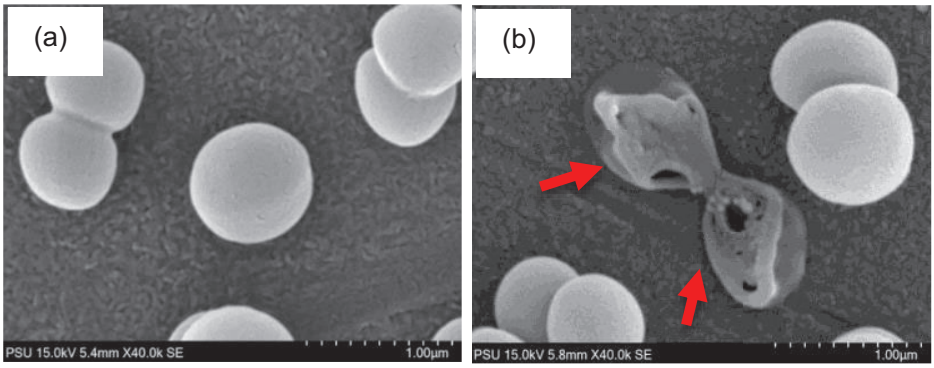

Figure 5: SEM images of the cell morphology of *S. aureus* (a) before and (b) after treatment with PLA/OC5/ZnO5

3.4 Color and Light Transmission

The appearance of the films, notably their color, was an important factor in food packaging materials because it affected their overall acceptability by consumers [35,36]. The color parameters (L*, a*, b*, and ΔE*) of the films are presented in Table 2. The incorporation of OC did not significantly change the L* value (lightness), while the further addition of ZnO increased the lightness of the nanocomposite films compared to neat PLA. Furthermore, the addition of TA did not affect the L* value in comparison to the PLA/OC5/ZnO5 film. The color of the nanocomposite films shifted toward green with increases in the a* value. Moreover, TA slightly increased the a* value compared to the PLA/OC5/ZnO5 film. The OC markedly increased the yellowish color of the PLA film, while the further addition of ZnO had a slight effect in this regard compared to the initial incorporation of OC into the film. However, the greatest intensity could be observed in the nanocomposite film with TA (PLA/OC5/ZnO5/TA10). The total color difference (ΔE*) increased when OC was added to the PLA film. The greatest ΔE* value occurred in the PLA/OC5 film, while the lowest value found in PLA/OC5/ZnO5.

Table 2: Apparent color and transmittance of PLA and its nanocomposite films

Sample	L*	a*	b*	ΔE*	$T_{600\ nm}$	$T_{280\ nm}$
PLA	89.15 ± 0.14^{b}	-1.30 ± 0.01^{a}	1.06 ± 0.04^{c}	3.76 ± 0.09^{b}	86.37 ± 0.39^{a}	63.42 ± 0.21^{a}
PLA/OC5	88.46 ± 0.07^{c}	-1.38 ± 0.03^{b}	1.52 ± 0.01^{b}	4.51 ± 0.02^{a}	51.32 ± 0.39^{b}	16.31 ± 0.21^{b}
PLA/OC5/ZnO5	92.53 ± 0.22^{a}	-1.80 ± 0.02^{c}	1.57 ± 0.05^{b}	1.26 ± 0.03^{d}	2.35 ± 0.07^{c}	1.19 ± 0.10^{c}
PLA/OC5/ZnO5/TA10	92.31 ± 0.08^{a}	-1.88 ± 0.01^{c}	3.87 ± 0.02^{a}	3.27 ± 0.06^{c}	1.34 ± 0.04^{d}	0.03 ± 0.01^{d}

Note: Different superscript letters in the same column indicate significant differences ($p < 0.05$).

The ultraviolet and visible (UV-Vis) light barrier property was a significant parameter with regard to food packaging film applications: it represented the appearance of food products and/or protects UV-sensitive products from nutrient loss or discoloration and light deterioration. Spectrophotometric measurements in the UV (200–400 nm) and visible light (400–750 nm) regions were carried out to verify if the OC and ZnO nanoparticles affected the light barrier property of the nanocomposite films. The spectrophotometric curves in the UV-Vis range for the neat PLA and nanocomposite film samples are presented in Fig. 6a. Specifically, the transmittance values at 600 nm (T_{600}) and 280 nm (T_{280}) were used to analyze the transparency and UV blocking capacity of the films, respectively (Table 2). The curves confirmed that the highest light transmittance occurred for the neat PLA film, with all other curves shifting to lower values after the addition of OC. The PLA/OC5/ZnO5 film exhibited the lowest transmittance, while the addition of TA slightly altered its light transmission. This effect might arise from the nanoparticle distribution hindering the passage of light [15]. The neat PLA film exhibited the highest light transmittance for both visible and UV light, with T_{600} = 86% and T_{280} = 63% ($p < 0.05$), respectively. PLA/OC5/ZnO5/TA10 displayed almost complete visible and UV light shielding; this was a desirable property in food packaging applications, specifically for protecting light-sensitive food products [37]. ZnO acted as an efficient UV radiation absorber because its electronic structure presented a wide optical band gap in the UV region (3.37 eV) [38,39], consistent with results reported in the literature [16]. This finding also corresponded to the visual observations (Fig. 6b), revealing the greater transparency of the PLA film compared to the nanocomposite film samples.

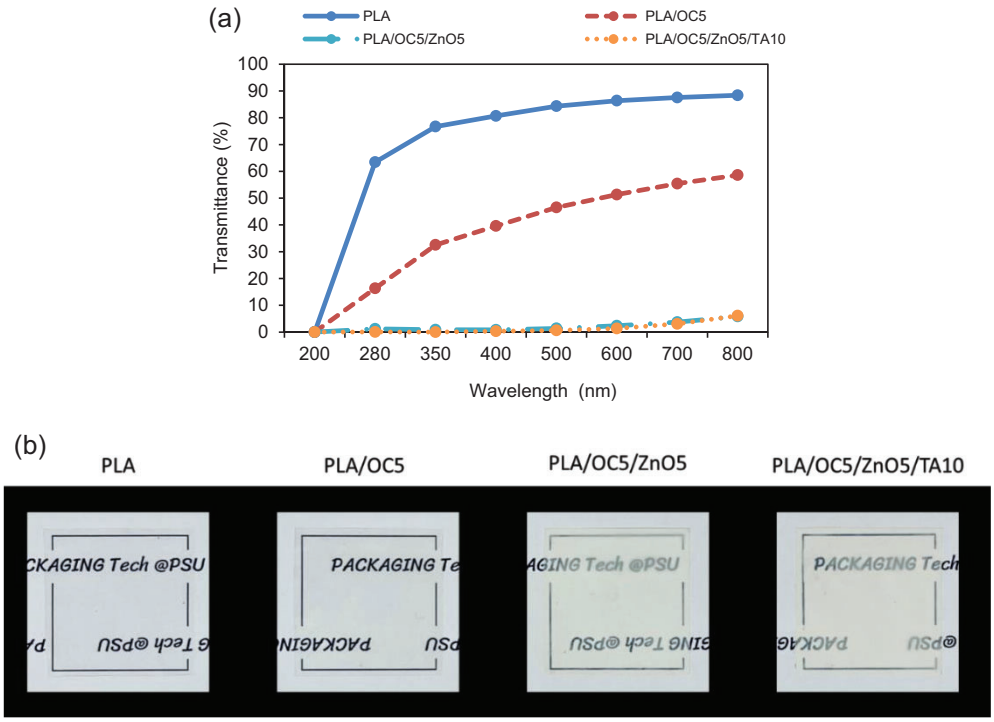

Figure 6: (a) UV-Vis spectra and (b) photographs of PLA and its nanocomposite films

3.5 Film Morphology

SEM was used to investigate the surface and cross-sectional morphology of PLA and its nanocomposite films (PLA/OC5, PLA/OC5/ZnO5, and PLA/OC5/ZnO5/TA10). According to the representative SEM micrographs in Fig. 7, a smooth and relatively flat surface without cracks or voids was observed for the neat PLA film. This morphology could be explained by the typical brittleness of PLA. The rough and heterogeneous surface structure observed in the nanocomposite films indicated that the OC and OC/ZnO particles were reasonably well dispersed in the PLA matrix. This led to an enhanced YM and water vapor barrier property, while the TS of the films was maintained compared to neat PLA. However, PLA/OC5 showed larger OC particles compared with the OC dispersed in the PLA/OC5/ZnO5 sample. The ZnO particles were evenly distributed in the PLA matrix, resulting in the formation of homogeneous nanocomposite films. The addition of TA slightly changed the film morphology compared to PLA/OC5/ZnO5. Such a compatibilization effect revealed the homogeneous dispersion and fine morphology of both the OC and ZnO in the TA-plasticized PLA film.

3.6 Differential Scanning Calorimetry (DSC)

From the DSC second heating scans and data presented in Fig. 8 and Table 3, PLA crystallization on heating was reduced for all nanocomposite films, as observed in the cold crystallization. The increase in T_{cc} and decrease in ΔH_{cc} indicated that the OC and ZnO particles did not act as nucleating agents to promote the rearrangement of the PLA chains during crystallization. Our finding was contrary to the results of some previous studies [6,40], while this behavior has been observed in other published works [7,41]. This could be explained by considering two opposing behaviors: the nano-fillers acted as nucleating sites, facilitating crystallization, while high miscibility between the organic modifier in the OC

and the PLA matrix simultaneously obstructed the flow during crystallization [7]. High miscibility between the OC or OC/ZnO and the PLA chains plausibly hindered the chain-folding and interchain interactions for crystal nuclei formation in both the plasticized and unplasticized samples.

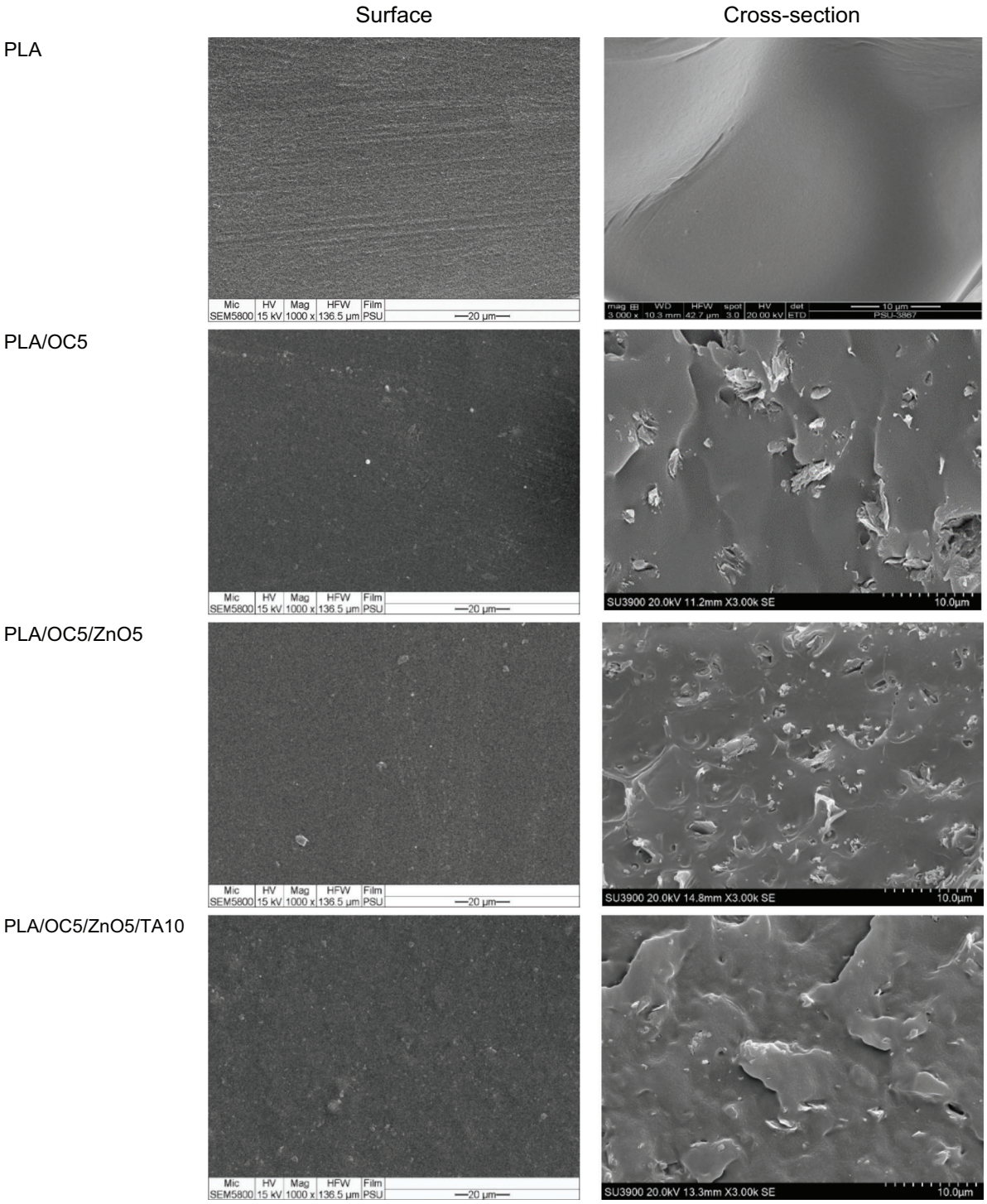

Figure 7: SEM images of the PLA film and its nanocomposites

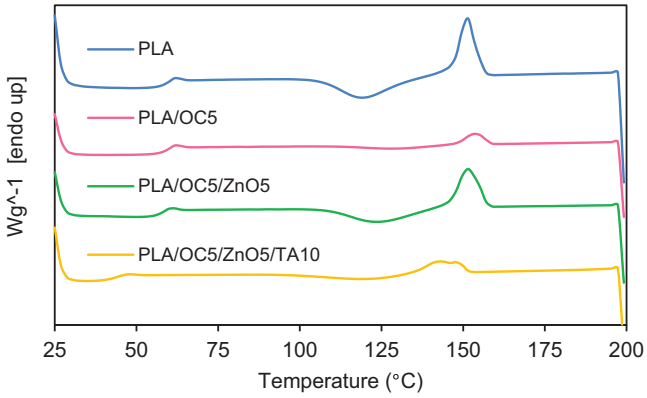

Figure 8: DSC thermograms of PLA and its nanocomposites

Table 3: DSC data of PLA and its nanocomposites

Sample	T_{cc} (°C)	ΔH_{cc} (J/g)	T_{m1} (°C)	T_{m2} (°C)	ΔH_m (J/g)	X_c (%)	T_g (°C)
PLA	119.17	19.87	151.17	–	24.10	4.55	59.02
PLA/OC5	128.00	2.81	153.50	–	5.33	2.85	58.82
PLA/OC5/ZnO5	123.83	16.64	151.50	–	19.13	2.97	56.95
PLA/OC5/ZnO5/TA10	119.00	7.18	148.17	143.00	8.55	1.84	42.76

The T_{m1} value of PLA did not show a marked change in the unplasticized nanocomposite films, though it decreased significantly in PLA/OC5/ZnO5/TA10. This suggested that the presence of TA molecules between the PLA chains resulted in the formation of a less perfect crystalline structure. The second peak of T_{m2} occurred at a lower temperature and represented the formation of a disordered crystalline form of PLA, as reported by Zhang et al. [42]. The X_c values of the PLA/OC5 and PLA/OC5/ZnO5 nanocomposites were lower than that of neat PLA, similarly observed by Atayev et al. [43]. These authors suggested that the reduction in X_c was due to the nano-fillers restricting crystalline growth, thereby slowing down the crystallization rate. Additionally, PLA/OC5/ZnO5/TA10 exhibited the lowest X_c; this arose from the plasticizing effect of TA, which increased the free volume and reduced the ability of the PLA chains to rearrange themselves and form crystallites [20]. According to the WVP results, the barrier property was enhanced regardless of the decreased crystallinity. This indicated that an extended tortuous path length, arising from the homogeneously dispersed OC or OC/ZnO, dominated the permeability coefficient instead of the crystallinity of PLA [43].

The incorporation of OC or OC/ZnO exhibited no relevant influence on the T_g of PLA, while a noticeable reduction occurred for PLA/OC5/ZnO5/TA10 due to the free volume increase arising from the TA plasticizing effect. Moreover, one T_g was observed, suggesting the miscibility of PLA with TA.

3.7 Thermal Gravimetric Analysis (TGA)

The thermal stability of films at elevated temperatures is commonly assessed by TGA. $T_{d,onset}$ was the initial weight loss temperature, and the maximum decomposition temperature (T_d) was determined from the temperature at the maximum peak in the first derivative mass loss (DTG) curve [44], as shown in Fig. 9 and Table 4. An initial weight loss at approximately 100°C corresponded to the loss of bound water in all film samples. A second major weight loss ($T_{d,onset}$) at around 333.56°C, 259.89°C, and 250.32°C and T_d values of approximately 357.78°C, 289.52°C, and 271.08°C were observed for PLA, PLA/OC5/ZnO5, and PLA/OC5/

ZnO5/TA10, respectively. The addition of ZnO could lead to stabilizing or degradation effects, as reported elsewhere [13]. However, the current experimental findings indicated that the incorporated ZnO reduced the thermal stability of PLA, in agreement with previously published works [15,39,45]. This decrease in thermal stability resulted from the fact that during the heating process, ZnO catalyzed PLA depolymerization, generating unzipping depolymerization and intermolecular transesterification reactions. Although the flexibility of the PLA/OC5/ZnO5/TA10 film improved markedly with the aid of TA as a plasticizer, its thermal stability was reduced owing to the increase in the free volume in the PLA chains [46].

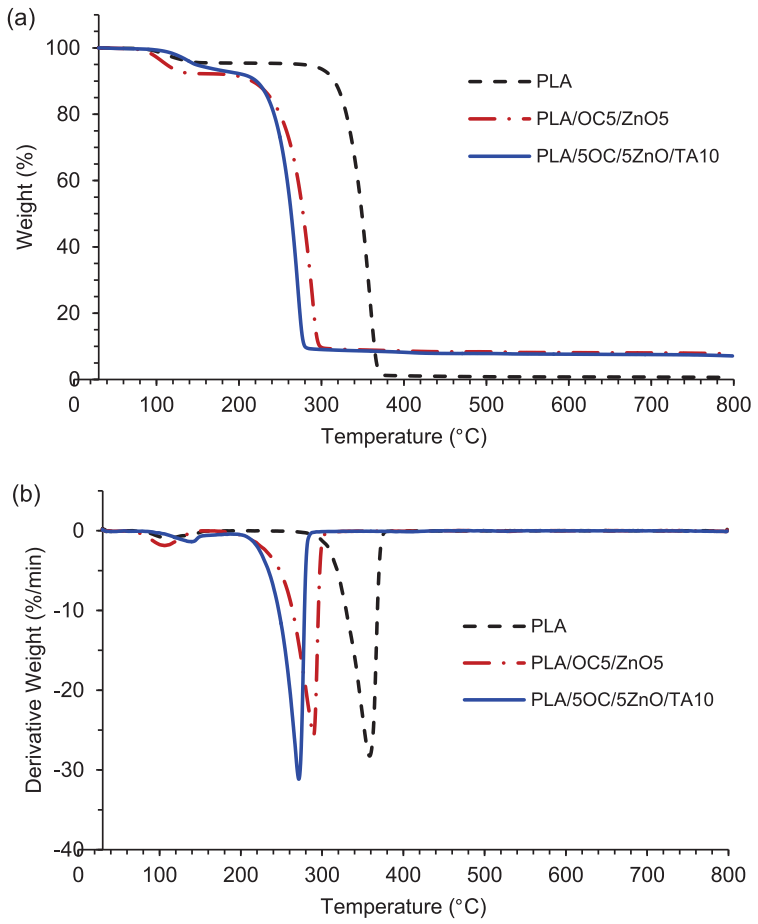

Figure 9: (a) TGA and (b) DTG thermograms of PLA and its nanocomposites

Table 4: Thermal characteristics of PLA and its nanocomposites

Samples	$T_{d,onset}$ (°C)	T_d (°C)
PLA	333.56	357.78
PLA/OC5/ZnO5	259.89	289.52
PLA/OC5/ZnO5/TA10	250.32	271.08

4 Conclusion

Novel sustainable eco-friendly PLA/OC/ZnO nanocomposite films notably suited to food packaging applications were successfully prepared, exhibiting good OC and ZnO dispersion. The synergism of OC and ZnO promoted a prominent improvement in both the UV-Vis light barrier and water vapor barrier properties of the films (with no deterioration in the YM and TS values) compared with the neat PLA and PLA/OC films. Moreover, the combination of OC and ZnO in PLA/OC5/ZnO5 led to the highest antibacterial activity against both the selected gram-positive and gram-negative foodborne bacteria; additionally, the antibacterial performance was time dependent. The flexibility of the film was effectively enhanced by adding the TA plasticizer. Considering their multifunctional properties (anti-UV-Vis, antibacterial, mechanical, water vapor permeability, etc.), such nanocomposite films could prove notably beneficial in the production of food packaging materials.

Acknowledgement: The authors were deeply grateful for the financial support, provided by Prince of Songkla University (PSU), Hat Yai, Songkhla, Thailand.

Funding Statement: Prince of Songkla University (PSU), Hat Yai, Songkhla, Thailand (Grant Number AGR581246S).

Author Contributions: The authors confirm contribution to the paper as follows: Conceptualization, supervision, writing-original draft preparation, review and editing, and funding acquisition: Ponusa Songtipya; Methodology: Theerarat Sengsuk; Formal analysis and investigation, supervision, and writing-review: Thummanoon Prodpran, Ladawan Songtipya. All authors reviewed the results and approved the final version of the manuscript.

Availability of Data and Materials: The data that support the findings of this study are available from the corresponding author, PS, upon reasonable request.

Conflicts of Interest: The authors declare that they have no conflicts of interest to report regarding the present study.

References

1. Sharma R, Jafari SM, Sharma S. Antimicrobial bio-nanocomposites and their potential applications in food packaging. Food Control. 2020;112:107086. doi:10.1016/j.foodcont.2020.107086.
2. Asgher M, Qamar SA, Bilal M, Iqbal HMN. Bio-based active food packaging materials: sustainable alternative to conventional petrochemical-based packaging materials. Food Res Intern. 2020;137:109625. doi:10.1016/j.foodres.2020.109625.
3. Taib NAAB, Rahman MR, Huda D, Kuok KK, Hamdan S, et al. A review on poly lactic acid (PLA) as a biodegradable polymer. Polym Bull. 2023;80(2):1179–213. doi:10.1007/s00289-022-04160-y.
4. Priyadarshi R, Roy S, Ghosh T, Biswas D, Rhim JW. Antimicrobial nanofillers reinforced biopolymer composite films for active food packaging applications—a review. Sustain Mater Technol. 2022;32:e00353.
5. Dharini V, Periyar Selvam S, Jayaramudu J, Sadiku Emmanuel R. Functional properties of clay nanofillers used in the biopolymer-based composite films for active food packaging applications—review. Appl Clay Sci. 2022;226:106555. doi:10.1016/j.clay.2022.106555.
6. Ogata N, Jimenez G, Kawai H, Ogihara T. Structure and thermal/mechanical properties of poly(/-lactide)-clay blend. J Polym Sci Part B Polym Phys. 1997;35(2):389–96. doi:10.1002/(ISSN)1099-0488.
7. Das K, Ray D, Banerjee I, Bandyopadhyay NR, Sengupta S, et al. Crystalline morphology of PLA/clay nanocomposite films and its correlation with other properties. J Appl Polym Sci. 2010;118(1):143–51. doi:10.1002/app.v118:1.
8. Ray SS, Okamoto M. Biodegradable polylactide and its nanocomposites: opening a new dimension for plastics and composites. Macromol Rapid Commun. 2003;24(14):815–40. doi:10.1002/marc.v24:14.

9. Kalendova A, Smotek J, Stloukal P, Kracalik M, Slouf M, Laske S. Transport properties of poly(lactic acid)/clay nanocomposites. Polym Eng Sci. 2019;59(12):2498–501. doi:10.1002/pen.v59.12.
10. Rhim JW, Hong SI, Ha CS. Tensile, water vapor barrier and antimicrobial properties of PLA/nanoclay composite films. LWT—Food Sci Technol. 2009;42(2):612–7. doi:10.1016/j.lwt.2008.02.015.
11. Chong WJ, Shen S, Li Y, Trinchi A, Pejak D, et al. Additive manufacturing of antibacterial PLA-ZnO nanocomposites: benefits, limitations and open challenges. J Mater Sci Technol. 2022;111:120–51. doi:10.1016/j.jmst.2021.09.039.
12. Marra A, Silvestre C, Duraccio D, Cimmino S. Polylactic acid/zinc oxide biocomposite films for food packaging application. Int J Biol Macromol. 2016;88:254–62. doi:10.1016/j.ijbiomac.2016.03.039.
13. Pantani R, Gorrasi G, Vigliotta G, Murariu M, Dubois P. PLA-ZnO nanocomposite films: water vapor barrier properties and specific end-use characteristics. Eur Polym J. 2013;49(11):3471–82. doi:10.1016/j.eurpolymj.2013.08.005.
14. De Silva RT, Pasbakhsh P, Lee SM, Kit AY. ZnO deposited/encapsulated halloysite-poly(lactic acid) (PLA) nanocomposites for high performance packaging films with improved mechanical and antimicrobial properties. Appl Clay Sci. 2015;111:10–20. doi:10.1016/j.clay.2015.03.024.
15. Yu F, Fei X, He Y, Li H. Poly(lactic acid)-based composite film reinforced with acetylated cellulose nanocrystals and ZnO nanoparticles for active food packaging. Int J Biol Macromol. 2021;186:770–9. doi:10.1016/j.ijbiomac.2021.07.097.
16. Boopasiri S, Sae-Oui P, Roamcharern N, Jangpromma N, Ngernyen Y, Siriwong C. A bio-plastic composite film based on nanocrystalline cellulose-zinc oxide reinforced poly(lactic acid) with enhanced UV-shielding effect and antibacterial activity for food packaging applications. Food Packag Shelf Life. 2023;38:1–12.
17. Rodolfo A Jr, Innocentini-Mei LH. Poly(vinyl chloride)/metallic oxides/organically modified montmorillonite nanocomposites: preparation, morphological characterization, and modeling of the mechanical properties. J Appl Polym Sci. 2010;116(1):422–32. doi:10.1002/app.v116:1.
18. Muiz LJ, Juwono AL, Krisnandi YK. A review: silver-zinc oxide nanoparticles—organoclay-reinforced chitosan bionanocomposites for food packaging. Open Chem. 2022;20(1):1155–70. doi:10.1515/chem-2022-0224.
19. YousefniaPasha H, Mohtasebi SS, Tabatabaeekoloor R, Taherimehr M, Javadi A, Soltani Firouz M. Preparation and characterization of the plasticized polylactic acid films produced by the solvent-casting method for food packaging applications. J Food Process Preserv. 2021;45(12):e16089.
20. Johar M, Zarkasi KZ, Zaini NAM, Rusli A. Enhancement of mechanical, rheological and antifungal properties of polylactic acid/ethylene-vinyl-acetate blend by triacetin plasticizer. J Polym Res. 2023;30(7):259. doi:10.1007/s10965-023-03630-9.
21. Kammoun R, Zmantar T, Ghoul S. Scanning electron microscopy approach to observe bacterial adhesion to dental surfaces. MethodsX. 2020;7:1–6.
22. Gomez-Gamez AB, Yebra-Rodriguez A, Peñas-Sanjuan A, Soriano-Cuadrado B, Jimenez-Millan J. Influence of clay percentage on the technical properties of montmorillonite/polylactic acid nanocomposites. Appl Clay Sci. 2020;198:105818. doi:10.1016/j.clay.2020.105818.
23. Giannakas A, Salmas C, Leontiou A, Tsimogiannis D, Oreopoulou A, Braouhli J. Novel LDPE/Chitosan rosemary and melissa extract nanostructured active packaging films. Nanomaterials. 2019;9(8):1105. doi:10.3390/nano9081105.
24. Bezerra Lima EM, Middea A, Marconcini JM, Corrêa AC, Fernandes Pereira J, et al. Biodegradable PLA based nanocomposites for packaging applications: the effects of organo-modified bentonite concentration. J Appl Polym Sci. 2021;138(36):50907. doi:10.1002/app.50907.
25. Alexandre M, Dubois P. Polymer-layered silicate nanocomposites: preparation, properties and uses of a new class of materials. Mater Sci Eng R Rep. 2000;28(1):1–63. doi:10.1016/S0927-796X(00)00012-7.
26. Sinha Ray S, Bousmina M. Biodegradable polymers and their layered silicate nanocomposites: in greening the 21st century materials world. Prog Mater Sci. 2005;50(8):962–1079. doi:10.1016/j.pmatsci.2005.05.002.
27. Sinha Ray S, Okamoto M. Polymer/layered silicate nanocomposites: a review from preparation to processing. Prog Polym Sci. 2003;28(11):1539–641. doi:10.1016/j.progpolymsci.2003.08.002.

28. Gupta GS, Senapati VA, Dhawan A, Shanker R. Heteroagglomeration of zinc oxide nanoparticles with clay mineral modulates the bioavailability and toxicity of nanoparticle in *Tetrahymena pyriformis*. J Colloid Interface Sci. 2017;495:9–18. doi:10.1016/j.jcis.2017.01.101.
29. Yano K, Usuki A, Okada A. Synthesis and properties of polyimide-clay hybrid films. J Polym Sci Part A: Polym Chem. 1997;35(11):2289–94. doi:10.1002/(ISSN)1099-0518.
30. Darie RN, Pâslaru E, Sdrobis A, Pricope GM, Hitruc GE, et al. Effect of nanoclay hydrophilicity on the poly(lactic acid)/clay nanocomposites properties. Ind Eng Chem Res. 2014;53(19):7877–90. doi:10.1021/ie500577m.
31. Bureš F. Quaternary ammonium compounds: simple in structure, complex in application. Top Curr Chem. 2019;377(3):1–21.
32. Roy A, Joshi M, Butola BS. Antimicrobial performance of polyethylene nanocomposite monofilaments reinforced with metal nanoparticles decorated montmorillonite. Colloids Surf B. 2019;178:87–93. doi:10.1016/j.colsurfb.2019.02.045.
33. Kumar R, Umar A, Kumar G, Nalwa HS. Antimicrobial properties of ZnO nanomaterials: a review. Ceram Int. 2017;43(5):3940–61. doi:10.1016/j.ceramint.2016.12.062.
34. Liang H, Wang H, Sun X, Xu W, Meng N, Zhou N. Development of ZnO/Ag nanoparticles supported polydopamine-modified montmorillonite nanocomposites with synergistic antibacterial performance. Appl Clay Sci. 2023;244:107112. doi:10.1016/j.clay.2023.107112.
35. Roy S, Ramakrishnan R, Goksen G, Singh S. Recent progress on UV-light barrier food packaging films—a systematic review. Innov Food Sci Emerg Technol. 2024;91:103550. doi:10.1016/j.ifset.2023.103550.
36. Videira-Quintela D, Martin O, Montalvo G. Recent advances in polymer-metallic composites for food packaging applications. Trends Food Sci Technol. 2021;109:230–44. doi:10.1016/j.tifs.2021.01.020.
37. Trifol J, Plackett D, Sillard C, Szabo P, Bras J, Daugaard AE. Hybrid poly(lactic acid)/nanocellulose/nanoclay composites with synergistically enhanced barrier properties and improved thermomechanical resistance. Polym Int. 2016;65(8):988–95. doi:10.1002/pi.5154.
38. Shanshool HM, Yahaya M, Yunus WMM, Abdullah IY. Investigation of energy band gap in polymer/ZnO nanocomposites. J Mater Sci: Mater Electron. 2016;27(9):9804–11. doi:10.1007/s10854-016-5046-8.
39. Lizundia E, Penayo MC, Guinault A, Vilas JL, Domenek S. Impact of ZnO nanoparticle morphology on relaxation and transport properties of PLA nanocomposites. Polym Test. 2019;75:175–84. doi:10.1016/j.polymertesting.2019.02.009.
40. Fukushima K, Tabuani D, Camino G. Poly(lactic acid)/clay nanocomposites: effect of nature and content of clay on morphology, thermal and thermo-mechanical properties. Mater Sci Eng: C. 2012;32(7):1790–5. doi:10.1016/j.msec.2012.04.047.
41. Gumus S, Ozkoc G, Aytac A. Plasticized and unplasticized PLA/organoclay nanocomposites: short- and long-term thermal properties, morphology, and nonisothermal crystallization behavior. J Appl Polym Sci. 2012;123(5):2837–48. doi:10.1002/app.v123.5.
42. Zhang J, Tashiro K, Tsuji H, Domb AJ. Disorder-to-order phase transition and multiple melting behavior of Poly(l-lactide) investigated by simultaneous measurements of WAXD and DSC. Macromolecules. 2008;41(4):1352–7. doi:10.1021/ma0706071.
43. Atayev P, Oner M. Effect of incorporation of clay and zinc oxide nanoparticles on oxygen barrier properties of polypropylene sheet. J Plast Film Sheeting. 2014;30(3):248–65. doi:10.1177/8756087913503652.
44. Da Silva LR, Da Silva LO, De Carvalho LH, De Oliveira AD, Bardi MAG, et al. Physical, morphological, structural, thermal and antimicrobial characterization of films based on Poly(Lactic Acid), organophilic montmorillonite and oregano essential oil. Mater Res. 2022;25:1–12.
45. Akshaykranth A, Jayarambabu N, Venkatappa Rao T, Rakesh Kumar R, Srinivasa Rao L. Antibacterial activity study of ZnO incorporated biodegradable poly(lactic acid) films for food packaging applications. Polym Bull. 2023;80(2):1369–84. doi:10.1007/s00289-022-04126-0.
46. Chen W, Chen H, Yuan Y, Peng S, Zhao X. Synergistic effects of polyethylene glycol and organic montmorillonite on the plasticization and enhancement of poly(lactic acid). J Appl Polym Sci. 2019;136(21):47576. doi:10.1002/app.47576.